A Power-Angle-Based Adaptive Overcurrent Protection Scheme for Grid-Forming Inverter Under Large Grid Disturbances

Huang, Liang; Wu, Chao; Zhou, Dao; Blaabjerg, Frede

Published in:
IEEE Transactions on Industrial Electronics

DOI (link to publication from Publisher):
10.1109/TIE.2022.3199906

Publication date:
2023

Document Version
Accepted author manuscript, peer reviewed version

A Power-Angle-Based Adaptive Overcurrent Protection Scheme for Grid-Forming Inverter Under Large Grid Disturbances

Liang Huang, *Student Member, IEEE*, Chao Wu, *Member, IEEE,* Dao Zhou, *Senior Member, IEEE,* and Frede Blaabjerg, *Fellow, IEEE*

***Abstract*—As the capacity of renewable energy generation increases, grid-forming (GFM) inverters are deemed as promising solutions for low inertia power grids. However, power-electronic-based inverters have limited overcurrent capability, so additional overcurrent protection schemes are necessary. More importantly, the stability should not be jeopardized by using additional overcurrent protection schemes. However, GFM inverters with the conventional current reference limiting method tend to be unstable under large grid disturbances such as grid frequency drop. To address this problem, this paper proposes a virtual power angle limiting method. The main idea of this method is to limit the output power by limiting the power angle instead of directly limiting the current reference. Thus, the power synchronization control law is still satisfied when the overcurrent protection is triggered, so that the stability can be maintained. Besides, after redesigning the power angle limiting value, the proposed method is suitable for grid voltage sag cases. A significant advantage of the proposed method is that the output current can be limited automatically during grid voltage sag or frequency drop events without the need of fault detection or tuning control structures and parameters. Simulation and experimental results have verified the effectiveness of the proposed method.**

***Index Terms*—grid forming inverter, overcurrent protection, virtual power angle limit, grid frequency drop, grid voltage sag.**

I. Introduction

In the past decades, due to the foreseen exhaustion of conventional fossil-based energies and their climate impact, many global efforts have been devoted to developing renewable energy sources, such as solar photovoltaic (PV) and wind power [1]. Thus, the proportion of converter-interfaced generators (CIGs) or inverter-based resources (IBRs) in power systems increases rapidly, especially in Europe [2]. Unlike traditional synchronous generators (SGs) having large overcurrent capability, i.e., 6-8 p.u. [3], power-electronic-based inverters have limited overcurrent capability, i.e., 1.5 p.u. [4]. Hence, an effective overcurrent protection scheme is important for grid-connected inverters [5].

For grid-following (GFL) inverters, due to the proportional relation between the output power and the current reference, the overcurrent protection can be easily fulfilled by directly limiting the current reference. Regardless that the current reference is limited or not, the phase-locked loop (PLL) can obtain the voltage phase angle at the point of common coupling (PCC) and keep synchronization with the grid. However, when this method is used for grid-forming (GFM) inverters, the system may lose synchronization under large grid disturbances, because when the current reference is limited, the power synchronization control law, (i.e., the proportional relation between the active power and the power angle) is destroyed [6]. In return, when the power synchronization control law is destroyed, the output active power and current cannot be controlled stably. Thus, the GFM inverter system has the risk of instability when the conventional current reference limiting method is used [7].

So far, there are many different GFM control schemes proposed in existing research [8], such as droop control [9], synchronverter [10], virtual synchronous generator (VSG) [11], power synchronization control [12], synchronous power control [13] and virtual oscillator control [14]. Among these schemes, the VSG or droop-based dual-loop voltage and current vector control scheme attracts more attention [15]-[20], where a virtual impedance or admittance is usually used to improve the small-signal stability under normal conditions [18]. However, the requirement of the overcurrent protection has not been considered in these studies.

To address the overcurrent problem, an easy way is to increase the physical overcurrent capability of inverters to be as high as that of SGs. But it is not economic to do so. Alternatively, from the control point of view, five possible current limiting solutions have been presented in existing literature. The first method is switching the control mode from GFM to GFL mode when the overcurrent event happens [21]. However, during the recovery process, the wind-up issue of the integrator may worsen the transient performance [22]. Besides, grid fault detection is necessary for switching the control modes [21]. The second method is using a large virtual impedance to reduce the inverter voltage reference [23]-[25]. Then, the output current can be limited in this way. However, the performance of this method is sensitive to the grid impedance, which may restrict its effectiveness when the short-circuit ratio (SCR) changes [26]. Besides, when the virtual impedance is changed suddenly, a transient process is inevitable, which may worsen the transient performance [25].

The third method is modifying the power reference according to the grid voltage during grid fault. Meanwhile, the current reference limiting method is still used [26]. This method may be effective under grid voltage sag conditions, but it is not effective under grid frequency drop conditions. This is because the output power of the droop-based GFM inverter not only depends on the power reference but also relies on the grid frequency. When the grid frequency is reduced, only limiting the power reference cannot prevent overcurrent. Aside from these three approaches, two approaches by adding a frequency feedforward term to the *P-f* droop controller is proposed in [27] and [28] recently. However, the method proposed in [27] is only suitable for the grid voltage sag case, while the method proposed in [28] is only suitable for the grid frequency drop case.

Different from these existing methods, this paper proposes a novel virtual power angle limiting method. The basic idea of this method is to restrict the output power by limiting the power angle instead of directly limiting the current reference. Thus, the output current can be restricted indirectly. By using this method, the power synchronization control law is still satisfied when the overcurrent protection is triggered, so that the synchronization stability (which means the rotor angle stability in the classification of power system stability) can be maintained. Overall, the main contribution of this paper is proposing a novel overcurrent protection scheme for the GFM inverter, which can make sure a stable equilibrium point still exists under large grid disturbances, so that the stability can be guaranteed. Besides, the advantages of the proposed method over existing methods can be summarized as follows:

1) The proposed overcurrent protection method is suitable for both grid frequency drop and grid voltage sag cases.

2) Automatic and seamless transition between normal and grid fault conditions is achieved by using the proposed method, which can improve the transient performance.

3) The proposed method can be adaptive to the grid voltage magnitude variation, so the fault detection is not necessary.

Referring to a standardized assessment framework for grid-connected inverter in [29], the grid frequency drop and the grid voltage sag are selected as large grid disturbances for test in this paper. Besides, both strong and weak grid conditions are used in each test case.

The rest of this paper is organized as follows. Section II reviews the instability mechanism of the conventional current reference limiting method. Then, the proposed novel overcurrent protection method is introduced in Section III. Simulation and experimental results are provided in Section IV. Finally, concluding remarks are drawn in Section V.

II. Instability Mechanism of Conventional Current Reference Limiting Method

A. Configuration of the study system

Schematic diagram of the conventional droop-based GFM inverter embedding current reference limit is presented in Fig. 1. To differentiate the variables in different frames, the subscripts "*abc*, *αβ*, and *dq*" of the variables represent the variables in different control frames. Besides, for clarity, the variables in **bold** stand for vectors in this paper.

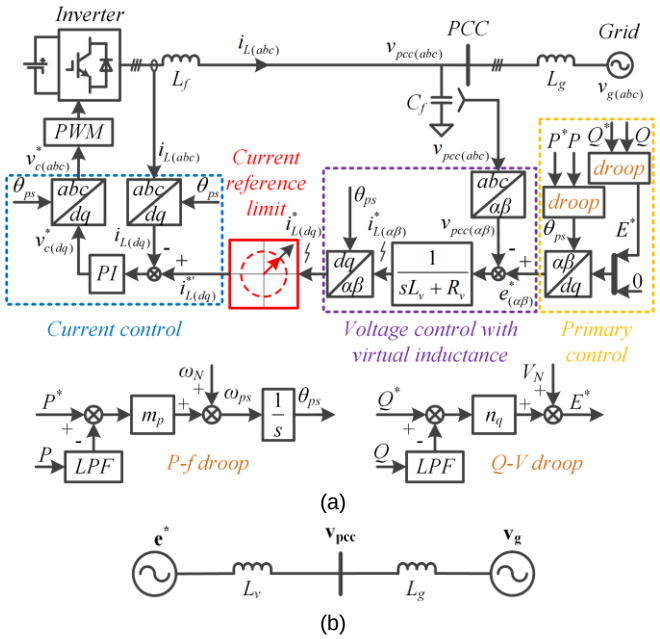

Fig. 1. Schematic diagram of conventional droop-based GFM inverter embedding current reference limit [26]. (a) Physical system and control scheme; (b) Equivalent circuit.

The physical system and control scheme of the droop-based GFM inverter is shown in Fig. 1(a), where $v_{g(abc)}$ is the grid voltage, $v_{pcc(abc)}$ is the output voltage at the PCC, and $e^*_{(\alpha\beta)}$ is the voltage reference generated by droop controllers. Besides, L_g is the grid inductance. L_f and C_f are the output filter inductance and capacitance. The typical *P-f* and *Q-V* droop controllers are used to control the active and reactive power. Besides, the typical proportional-integral (PI) control is used for the current control [18], [26]. Notably, a virtual inductance and a virtual resistance is included in the voltage control, which can be achieved by the virtual admittance approach [18], [26]. In order to realize power decoupling control, the virtual inductance L_v is designed much larger than the virtual resistance R_v [30]. Thus, the virtual resistance is ignored in this paper. Same as [18], the virtual inductance L_v is designed as 0.5 p.u. to make sure the GFM inverter has good small-signal stability under normal operating conditions. Moreover, the current reference limiting method is the same as [26], which is marked in red in Fig.1. The limiting expression of this method is given by (1), and the limiting value is set as the maximum current I_{max}.

$$i^{*'}_{L(dq)} = \begin{cases} i^*_{L(dq)}, & \text{if } \sqrt{{i^*_{Ld}}^2 + {i^*_{Lq}}^2} < I_{max} \\ i^*_{L(dq)} \cdot \dfrac{I_{max}}{\sqrt{{i^*_{Ld}}^2 + {i^*_{Lq}}^2}}, & \text{otherwise} \end{cases} \tag{1}$$

It can be seen from (1) that when the magnitude of the current vector $\mathbf{i}^*_L$ is lower than the limiting value I_{max}, the limiter does not work. Reversely, when the magnitude of the vector $\mathbf{i}^*_L$ is larger than I_{max}, the limiter works. In this case, the magnitude of the vector $\mathbf{i}^*_L$ is limited to I_{max}, and the phase angle of the vector $\mathbf{i}^*_L$ is kept invariable [26].

Besides, the equivalent circuit of the study system is shown in Fig. 1(b), where L_v is the virtual inductance.

B. Instability mechanism of the conventional current reference limiting method

First of all, in order to understand the problem of the current reference limiting method, the instability mechanism analysis presented in [6] is reviewed. The voltage and current vector diagrams of the grid-connected system are shown in Fig. 2, where δ is the angle between vectors $\mathbf{e}^*$ and $\mathbf{v_g}$, and ϕ is the angle between vectors $\mathbf{e}^*$ and $\mathbf{i_L}$. As shown in Fig. 2(a), when the current limiter is unsaturated (normal conditions), the output power of the GFM inverter depends on two voltage vectors $\mathbf{e}^*$ and $\mathbf{v_g}$. In this case, the output power meets the well-known *P*-δ equation given by (2). Moreover, as shown in Fig. 2(b), when the current limiter is saturated (overcurrent conditions), the GFM inverter can be considered as a current source with a constant magnitude. Thus, the output power of the GFM inverter depends on the vectors $\mathbf{i_L}$ and $\mathbf{v_g}$. In this case, equation (2) is not satisfied anymore. Instead, the expression of the output power can be rewritten as (3).

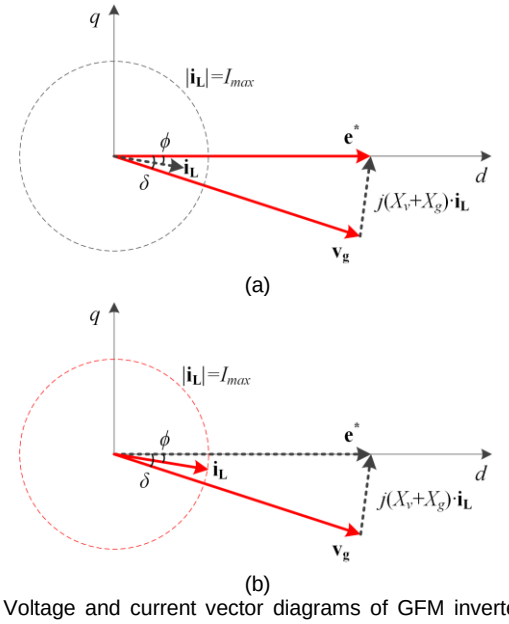

Fig. 2. Voltage and current vector diagrams of GFM inverter in two cases of current limiter. (a) Unsaturated case; (b) Saturated case.

$$P = \frac{3}{2} \cdot \frac{E^* \cdot V_g}{X_v + X_g} \cdot \sin(\delta) \tag{2}$$

where E^* and V_g are the magnitudes of the vectors $\mathbf{e}^*$ and $\mathbf{v_g}$.

$$P = \frac{3}{2} \cdot I_{max} \cdot V_g \cdot \cos(\delta - \phi) \tag{3}$$

Same as [6], the angle ϕ in Fig. 2 is assumed very small for qualitative analysis. Thus, according to (2) and (3), theoretical operating trajectories of the GFM inverter under grid frequency drop conditions are shown in Fig. 3. As shown in Fig. 3(a), the operating trajectory follows the *P*-δ curve A-B-C-D in the case without any limit. It is assumed that the current magnitude reaches the maximum value I_{max} at point B. When the grid frequency is dropped from f_{o1} to f_{o2}, the operating point is changed from O_1 to O_2. Thus, the output current magnitude is higher than I_{max}. In this case, the system is stable but overcurrent. To limit the output current, a typical method is to limit the current reference. As shown in Fig. 3(b), the operating trajectory follows the curve A-B-E-F in the case with the current reference limit. When the grid frequency is dropped from f_{o1} to f_{o2}, there is no equilibrium point on the *P*-δ operating trajectory. In this case, the system is unstable. To solve this instability problem, a new overcurrent protection idea is proposed in this paper. As shown in Fig. 3(c), if the power angle can be limited to δ_{lim}, the output power can be limited to P_{o2}' when the grid frequency is changed to f_{o2}. Thus, the operating trajectory can stay at point B. Namely, the point O_2' is the final stable equilibrium point. The implementation of this new idea will be introduced in Section III.

III. Proposed Overcurrent Protection Scheme

To solve the instability problem caused by the current reference limiting method, a novel overcurrent protection scheme will be introduced in this section.

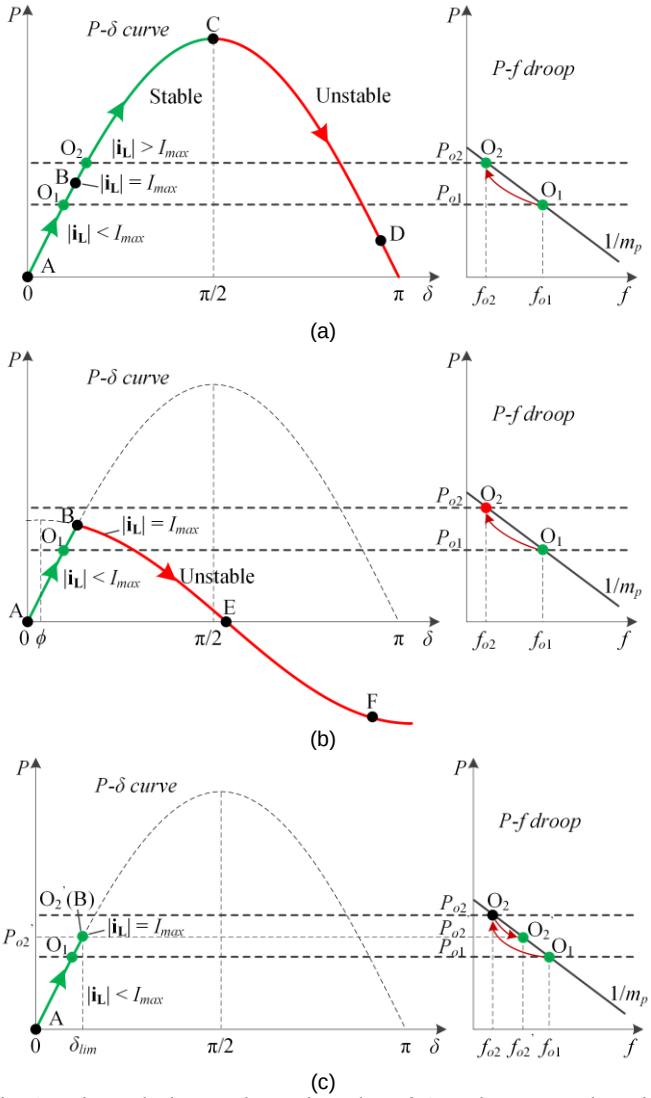

Fig. 3. Theoretical operating trajectories of GFM inverter under grid frequency drop conditions. (a) Without any limit; (b) With current reference limit; (c) With power angle limit.

A. Proposed virtual power angle limiting method

The voltage vector diagram of the GFM inverter with virtual inductance is shown in Fig. 4. Considering the grid voltage $\mathbf{v_g}$ and grid inductance X_g are usually unknown, the

real power angle δ is difficult to be obtained. Thus, the power angle δ cannot be directly used for implementing power limitation. However, a virtual power angle δ_v is known, which is equal to the angle difference θ_{ps} - θ_{pll}. Notably, θ_{ps} is the phase angle of the voltage vector $\mathbf{e}^*$, which is generated by the *P-f* droop controller. Besides, θ_{pll} is the phase angle of the voltage vector $\mathbf{v}_{pcc}$, which can be obtained by using a PLL.

Based on the above analysis, the proposed virtual power angle limiting method is shown in Fig. 5, where a PLL is used to obtain the phase angle of the PCC voltage. The limiting expression of the virtual power angle is given by (4). It can be seen that the virtual power angle limit block in Fig. 5 is transparent under normal conditions (namely, $\delta_v^{'} = \delta_v$ and $\theta_{ps}^{'} = \theta_{ps}$). But under overcurrent conditions, the angle $\delta_v^{'}$ is equal to the limiting value $\delta_{v(lim)}$. The design of the limiting value $\delta_{v(lim)}$ will be introduced in the following section.

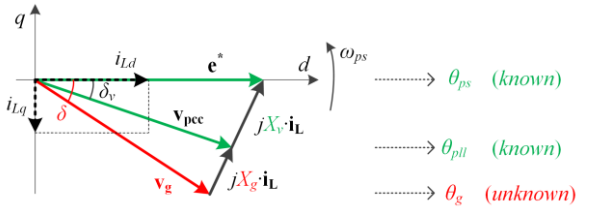

Fig. 4. Voltage and current vector diagrams of GFM inverter in d-q control frame.

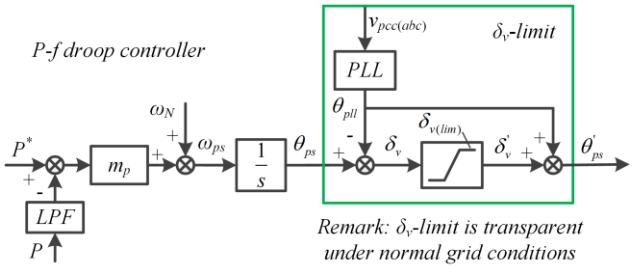

Fig. 5. Proposed virtual power angle limiting method.

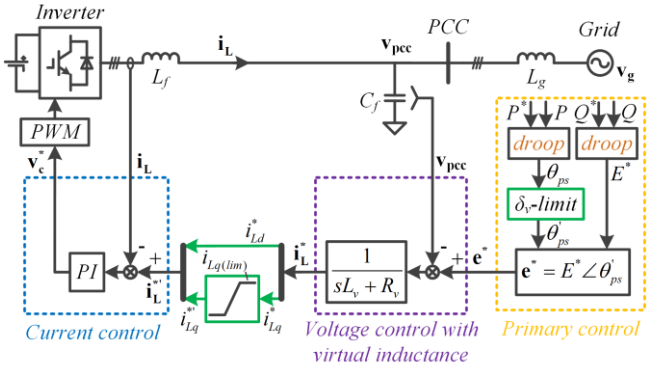

Fig. 6. Proposed overcurrent protection scheme for GFM inverter.

$$\delta_v^{'} = \min(\delta_{v(lim)}, \delta_v) \tag{4}$$

B. Design of virtual power angle limiting value

According to the voltage vector diagram in Fig. 4, the relationship between the active power *P* and the virtual power angle δ_v meets the *P*-δ equation given by (5).

$$P = \frac{3}{2}\cdot\frac{E^*\cdot V_{pcc}}{X_v}\cdot\sin(\delta_v) \tag{5}$$

where E^* and V_{pcc} are the magnitudes of vectors $\mathbf{e}^*$ and $\mathbf{v}_{pcc}$.

Thus, the expression of the virtual power angle δ_v can be derived as:

$$\delta_v = \arcsin\left(\frac{P}{\frac{3}{2}\cdot\frac{E^*\cdot V_{pcc}}{X_v}}\right) \tag{6}$$

Moreover, based on the voltage and current vector diagram in Fig. 4, it is known that the relationship between the active power *P* and the *d*-axis component current i_{Ld} meets (7).

$$P = \frac{3}{2}\cdot E^*\cdot i_{Ld} \tag{7}$$

Substituting (7) into (6), the expression of the virtual power angle δ_v can be derived as:

$$\delta_v = \arcsin\left(\frac{X_v\cdot i_{Ld}}{V_{pcc}}\right) \tag{8}$$

Thus, the limiting value $\delta_{v(lim)}$ can be calculated as:

$$\delta_{v(lim)} = \arcsin\left(\frac{X_v\cdot i_{Ld(lim)}}{V_{pcc}}\right) \tag{9}$$

where $i_{Ld(lim)}$ is the designed limiting value of the *d*-axis component current i_{Ld}.

Considering that the maximum current I_{max} of the inverter is usually designed between 1 p.u. and 1.2 p.u., I_{max} = 1 p.u. is chosen as an example for study in this paper. Besides, to remain some reactive power output capability in weak grids, the *d*-component limiting value $i_{Ld(lim)}$ is set as 0.9 p.u. in this paper. Notably, $i_{Ld(lim)}$ = 0.9 p.u. is just used as an example in this paper. It can also be designed as other values (e.g., 0.9 ~ 0.95 p.u.), which depends on the specific study case.

In addition, to make sure the magnitude of the output current is not higher than I_{max}, the *q*-component current can be limited by $i_{Lq(lim)}$ in (10), where the limiting expression is given by (11). Thus, the proposed overcurrent protection scheme for GFM inverter is shown in Fig. 6, where the differences between Fig. 6 and Fig. 1 are marked in green. For brevity, the coordinate transformations between different frames are omitted in Fig. 6, which are same as that in Fig. 1.

$$i_{Lq(lim)} = \sqrt{I_{max}^{\ 2} - i_{Ld}^{*\ 2}} \tag{10}$$

$$i_{Lq}^{*'} = \begin{cases} \min(i_{Lq(lim)}, i_{Lq}^*), & \text{if } i_{Lq}^* > 0 \\ \max(-i_{Lq(lim)}, i_{Lq}^*), & \text{otherwise} \end{cases} \tag{11}$$

where $i_{Lq(lim)}$ and -$i_{Lq(lim)}$ are upper and lower bounds of limiter.

It can be seen from Fig. 6 that the reactive power is not limited directly. However, when i_{Lq}^* is limited, the reactive power can be limited indirectly.

Based on the above analysis, the proposed virtual power angle limiting method can restrict the output power and current under frequency drop conditions. However, it still might be unstable under grid voltage sag conditions, because when the grid voltage magnitude is extremely low, there will be no equilibrium point. To make the proposed method effective under grid voltage sag conditions, the virtual power angle limiting value in (9) needs to be redesigned further.

C. Improved virtual power angle limiting value for grid voltage sag condition

According to (2), it is known that the output power *P* is proportional to the grid voltage magnitude V_g. Thus, when the

grid voltage magnitude V_g is reduced, the output power P is reduced as well. Hence, in the case of grid voltage sag, the inverter may not be able to provide enough power to the grid. Thus, appropriate power reduction is necessary, which can make a stable equilibrium point exist.

Theoretical operating trajectories of GFM inverter under grid voltage sags are shown in Fig. 7. As shown in Fig. 7(a), when the grid voltage magnitude is reduced from V_{g0} to V_{g1}, the operating trajectory is changed from A-B-C-D to A-B'-C'-D'. Thus, although the output power can be limited to P_{lim}, there is no equilibrium point on the trajectory A-B'-C'-D', because the maximum output power at point C' is still lower than the power limit P_{lim}.

To avoid the instability problem caused by grid voltage sag, a reasonable way is to modify the active power limiting value according to the grid voltage magnitude, such as "$P_{lim}^{new} = P_{lim} \cdot V_{g(\text{p.u.})}$" [26]. As shown in Fig. 7(b), when the active power limiting value is modified to P_{lim}^{new}, there is a stable equilibrium point B' after the grid voltage is reduced. Thus, the system is still stable. Similarly, since the output power P is proportional to the PCC voltage magnitude according to (4), the active power limiting value can also be modified depending on the PCC voltage, such as "$P_{lim}^{new} = P_{lim} \cdot V_{pcc(\text{p.u.})}$".

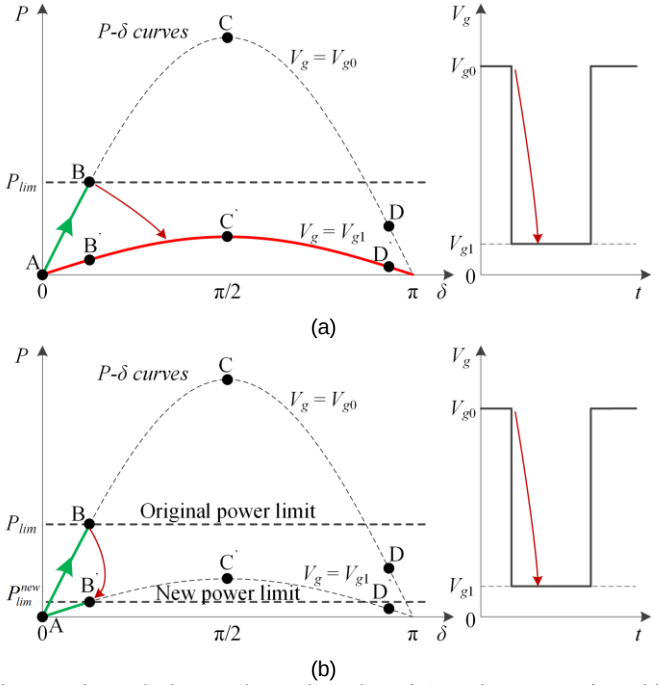

Fig. 7. Theoretical operating trajectories of GFM inverter under grid voltage sag conditions. (a) Initial limiting method; (b) Improved limiting method.

Moreover, considering the d-component current i_{Ld} is proportional to the active power P according to (6), modifying the d-component current limiting value is equivalent to modifying the active power limiting value. Thus, the limiting value $i_{Ld(lim)}$ can be redesigned as:

$$i_{Ld(lim)}^{new} = i_{Ld(lim)} \cdot V_{pcc(p.u.)} \tag{12}$$

According to (12), the virtual power angle limiting value in (9) can be redesigned as:

$$\delta_{v(lim)}^{new} = \arcsin\left(\frac{X_v \cdot i_{Ld(lim)} \cdot V_{pcc(p.u.)}}{V_{pcc}}\right) \tag{13}$$

According to the p.u. value expression "$V_{pcc(\text{p.u.})} = V_{pcc}/V_N$", (13) can be rewritten as (14).

$$\delta_{v(lim)}^{new} = \arcsin\left(\frac{X_v \cdot i_{Ld(lim)}}{V_N}\right) \tag{14}$$

where V_N is the rated voltage of the inverter.

Comparing (14) with (13), it can be seen that the PCC voltage is canceled, so the new limiting value $\delta_{v(lim)}^{new}$ in (14) only depends on the constant parameters X_v, V_N, and $i_{Ld(lim)}$. Therefore, it is not necessary to change $\delta_{v(lim)}^{new}$ in any cases. Notably, although $\delta_{v(lim)}^{new}$ is constant, P_{lim}^{new} can be adaptive to the grid voltage magnitude variation, as shown in Fig. 7(b). Thus, additional fault detection can be avoided to use.

D. Analysis of q-component current reference limiter and its impact on stability

As aforementioned, a q-component current reference limiter is used in the proposed control scheme. Its impact on stability and control will be briefly discussed in this section.

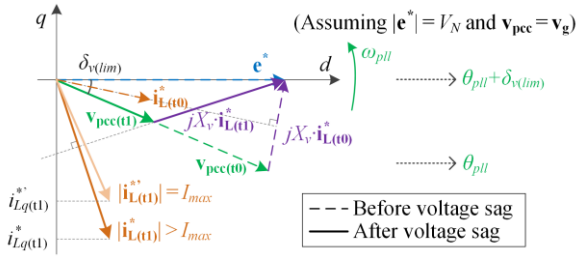

Fig. 8. Voltage and current vector diagrams of GFM inverters with the proposed control scheme under grid voltage sag conditions.

The voltage and current vector diagrams of GFM inverters with the proposed control scheme under grid voltage sag conditions are shown in Fig. 8. To simplify the analysis, assuming that $|\mathbf{e}^*|$ is constant and $\mathbf{v}_{pcc}$ is the same as $\mathbf{v}_g$. It can be seen from Fig. 8 that when the proposed δ_v-limiter is triggered, the power angle is limited to $\delta_{v(lim)}$. Thus, the P-f droop controller does not work anymore. Instead, the PLL is used for synchronization. When the PCC voltage is changed from $\mathbf{v}_{pcc(t0)}$ to $\mathbf{v}_{pcc(t1)}$, the current reference is changed from $\mathbf{i}^*_{L(t0)}$ to $\mathbf{i}^*_{L(t1)}$. Due to a large q-component, the magnitude of $\mathbf{i}^*_{L(t1)}$ is larger than I_{max}. When a q-component current reference limiter is used, a new current reference $\mathbf{i}^{*'}_{L(t1)}$ outputs from the limiter. Notably, since $\mathbf{e}^*$, $\delta_{v(lim)}$, and X_v are constant, as long as $\mathbf{v}_{pcc(t1)}$ is invariable, the output of the voltage controller (i.e., $\mathbf{i}^*_{L(t1)}$) is constant. Thus, the voltage control cannot be influenced by the current control. On the other hand, since the PLL is used for synchronization, which is unrelated to the voltage and power control, the current control in the synchronous d-q frame is also not influenced by the voltage control. Therefore, no matter whether the current reference is $\mathbf{i}^*_{L(t1)}$ or $\mathbf{i}^{*'}_{L(t1)}$, the current control loop can follow the reference. So, the q-component current reference limiter does not worsen the stability of the proposed method.

E. Comparison of overcurrent protection methods

In order to clarify the advantage of the proposed method, a comparison with existing overcurrent protection methods will be briefly discussed. The advantages and disadvantages of five existing methods are compared in Table I, where five indicators are selected for comparison.

TABLE I
COMPARISON OF ADVANTAGES AND DISADVANTAGES OF DIFFERENT OVERCURRENT PROTECTION METHODS

Methods	No need of grid fault detection	Smooth transition between normal and fault cases	Not sensitive to grid impedance or SCR variation	Effective in voltage sag case	Effective in frequency drop case
Control-mode-switching method [21]	No	No	Yes	Yes	Yes
Virtual impedance method [23]-[25]	Yes	No	No	Yes	Yes
Modifying power reference method [26]	No	Yes	Yes	Yes	No
Voltage-based frequency feedforward [27]	Yes	Yes	Yes	Yes	No
Power-based frequency feedforward [28]	Yes	Yes	Yes	No	Yes
Proposed method in this paper	Yes	Yes	Yes	Yes	Yes

To the best knowledge of the authors, five overcurrent protection methods for GFM inverters have been proposed in existing literature to address the instability problem caused by the current reference limiting method. However, each method has its own limitations.

The first method is the control-mode-switching method. The main idea is to switch the control mode from the GFM mode to the GFL mode when the grid fault happens. When the fault is clear, the control mode is switched back to the GFM mode. However, grid fault detection is necessary for this method, which may increase the complexity. Besides, during the recovery process, the wind-up issue of the integrator may worsen the transient performance [22].

The second method is the virtual impedance method. The main idea of this method is adding a large virtual impedance between the converter and the grid, so that the output current can be limited in this way. However, the performance of this method is sensitive to the grid impedance [26]. Besides, the virtual impedance is changed suddenly when the grid fault happens or ends. Thus, a transient oscillation process is inevitable [25].

The third method is modifying the power reference method. The main idea of this method is reducing the power reference when the grid fault happens. However, this method is not effective in the frequency drop case. Besides, the grid fault detection is necessary for this method.

The fourth method is the voltage-based frequency feedforward method. This method makes use of the *q*-component voltage to add a frequency feedforward term to the *P-f* droop controller. However, although this method is effective in the grid voltage sag case, it is not effective in the frequency drop case.

The fifth method is the power-based frequency feedforward method. Based on the value of the active power, a frequency feedforward term is added to the *P-f* droop controller. However, although this method is effective in the frequency drop case, it is not effective in the grid voltage sag case.

As shown in Table I, compared with these five existing methods, the proposed overcurrent protection method has more advantages than any one of these five existing methods. Specifically, the proposed method is effective for both grid voltage sag and grid frequency drop cases. Besides, it is not sensitive to the SCR variation. Moreover, smooth transition between normal and fault cases can be achieved by using the proposed method. Last but not least, since the proposed method can be adaptive to the grid voltage magnitude variation, additional fault detection is not necessary.

IV. SIMULATION AND EXPERIMENTAL VERIFICATION

A. Simulation verification

In order to verify the effectiveness of the proposed power-angle-based overcurrent protection scheme, a time-domain simulation model of GFM inverter is built in Matlab/Simulink.

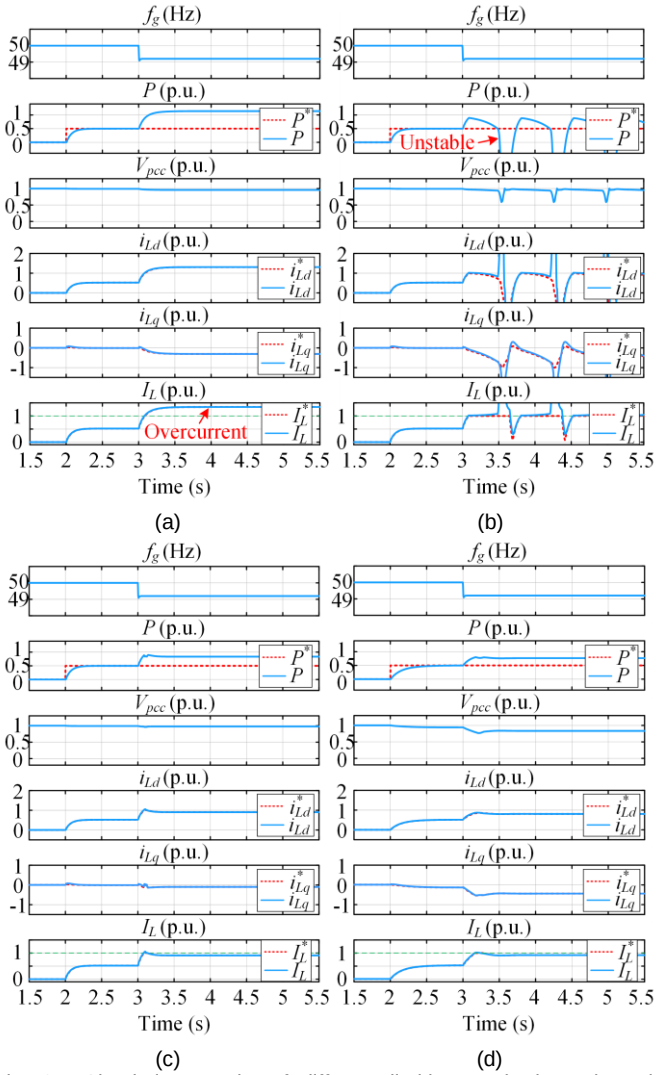

Fig. 9. Simulation results of different limiting methods under grid frequency drop conditions. (a) Without any limit, SCR = 15; (b) With current reference limiting method, SCR = 15; (c) With proposed virtual power angle limiting method, SCR = 15; (d) With proposed virtual power angle limiting method, SCR = 1.5.

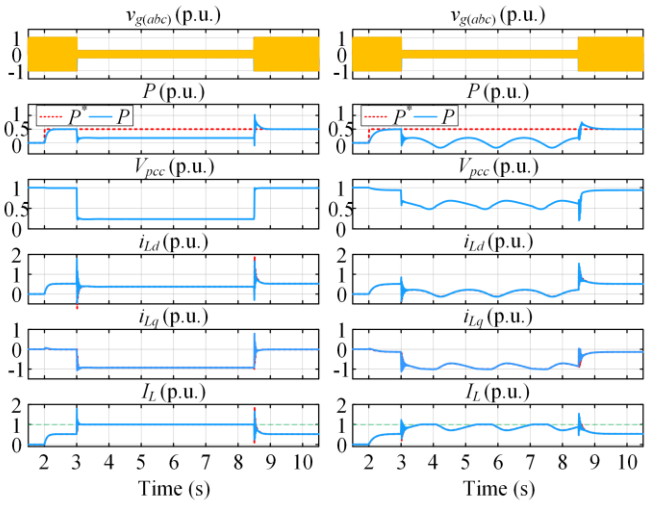

Fig. 10. Simulation results by using proposed virtual power angle limiting method under grid voltage sag conditions. (a) SCR = 15; (b) SCR = 1.5.

TABLE II
PARAMETERS OF GRID-FORMING INVERTER

	Parameters	Values
V_g	Grid phase voltage, peak value	50 V (1 p.u.)
f_g	Grid frequency	50 Hz (1 p.u.)
V_N	Rated voltage, peak value	50 V (1 p.u.)
ω_N	Rated angular frequency	2π·50 rad/s (1 p.u.)
P_N	Rated active power (3 phase)	800 W (1 p.u.)
S_N	Rated apparent power (3 phase)	800 VA (1 p.u.)
I_{max}	Rated/maximum current, peak value	10.6 A (1 p.u.)
V_{dc}	Input DC voltage	600 V
f_s	Switching/sampling frequency	10 kHz
L_f	Output filter inductor	3 mH (0.2 p.u.)
C_f	Output filter capacitor	10 μF (0.015 p.u.)
SCR	Short-circuit ratio	15 ~ 1.5
L_g	Grid inductor	1 ~ 10 mH
ω_i	Designed current-loop bandwidth	2000 rad/s
L_v	Virtual inductance	0.5 p.u.
R_v	Virtual resistance	0.05 p.u.
$i_{Ld(lim)}$	Limit value of d-component current	0.9 p.u.
m_p	Active power droop coefficient	2.5% ω_N/P_N
n_q	Reactive power droop coefficient	10% V_N/P_N
ω_{LPF}	Cut-off angular frequency of the LPFs	200 rad/s
ζ	Damping ratio of PLL	1
ω_n	Natural angular frequency of PLL	20 rad/s

To avoid the influence of high-frequency harmonics, the average model of the inverter is used in simulations, while the actual switching model is utilized in experiments. The system and control parameters are shown in Table II, which are also used for experiments. The simulation results of the different cases are shown in Fig. 9 and Fig. 10.

The simulation results by using different limiting methods under grid frequency drop conditions are shown in Fig. 9. The simulation results under strong grid condition with SCR = 15 are compared in Fig. 9(a)-(c). Initially, the power reference is given to be 0.5 p.u. The frequency drop happens at the instant of 3s. Fig. 9(a) shows the natural *P-f* droop response without any limit. When the grid frequency f_g is dropped from 50 Hz to 49.2 Hz, the active power is increased to be higher than 1 p.u., which leads to an overcurrent scenario. In this case, the system is stable, but overcurrent problems exist, which agrees well with the theoretical analysis in Fig. 3(a). Moreover, as shown in Fig. 9(b), when the conventional current reference limiting method is used, the magnitude of the current reference can be limited within 1 p.u. However, the output active power and current cannot be controlled stably. Namely, the system is unstable, which is consistent with the theoretical analysis in Fig. 3(b). Differently, as shown in Fig. 9(c), when the proposed virtual power angle limiting method is used, the output current magnitude can be limited within 1 p.u. stably, which also agrees with the theoretical analysis in Fig. 3(c). Besides, a weak grid condition with SCR = 1.5 is further used to test the effectiveness of the proposed method. As shown in Fig. 9(d), the output current magnitude can also be limited effectively under weak grid conditions.

In addition, the simulation results of the proposed method under grid voltage sag conditions are shown in Fig. 10, where the grid voltage magnitude is reduced from 1 p.u. to 0.2 p.u. for 5.5 seconds. A strong grid case with SCR = 15 is shown in Fig. 10(a), while a weak grid case with SCR = 1.5 is presented in Fig. 10(b). It can be seen in both strong and weak grid cases, the current magnitude can be limited within 1 p.u. effectively by using the proposed method.

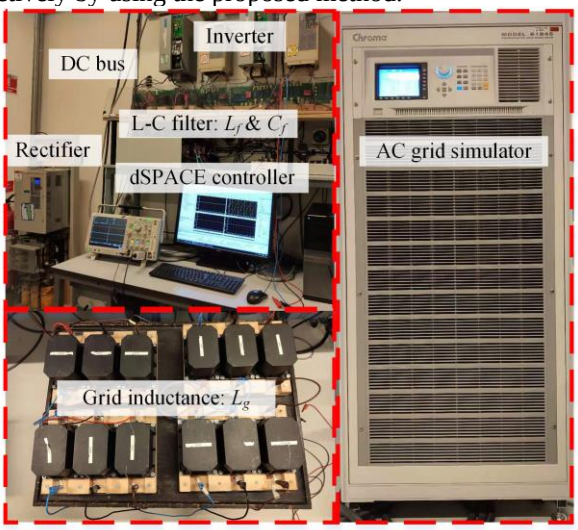

Fig. 11. View of experimental setup based on a dSPACE control system.

B. Experimental verification

As shown in Fig. 11, the experimental setup is established to verify the effectiveness of the proposed method. The infinite grid is realized by a grid simulator Chroma 61845. Different grid strengths are achieved by changing the grid inductance L_g. The grid-connected inverter is implemented by using the Danfoss FC103P11KT11 and the control algorithms are implemented by using the dSPACE1007. The circuit and control parameters are same as the parameters in Table II. Notably, due to having limited inductors in the laboratory, the grid voltage amplitude is intentionally reduced to create a weak grid condition with limited inductors.

The experimental results by using different current limiting methods under grid frequency drop conditions are shown in Fig. 12, where a strong grid condition with SCR = 15 is used. Like the simulation, the initial power reference is given to be 0.5 p.u. Fig. 12(a) shows the natural *P-f* droop response without any limit. When the grid frequency f_g is reduced from

50 Hz to 49.2 Hz, the output current magnitude increases to around 1.3 p.u. In this case, the system is stable, but overcurrent problems exist. Moreover, as shown in Fig. 12(b), when the conventional current reference limiting method is used, the system is unstable, which matches the simulation results in Fig. 9(b). A similar instability phenomenon has been reported in recent study [31]. Differently, as shown in Fig. 12(c), when the proposed method is used, the output current can be limited within 1 p.u. stably, which agrees with the simulation results in Fig. 9(c).

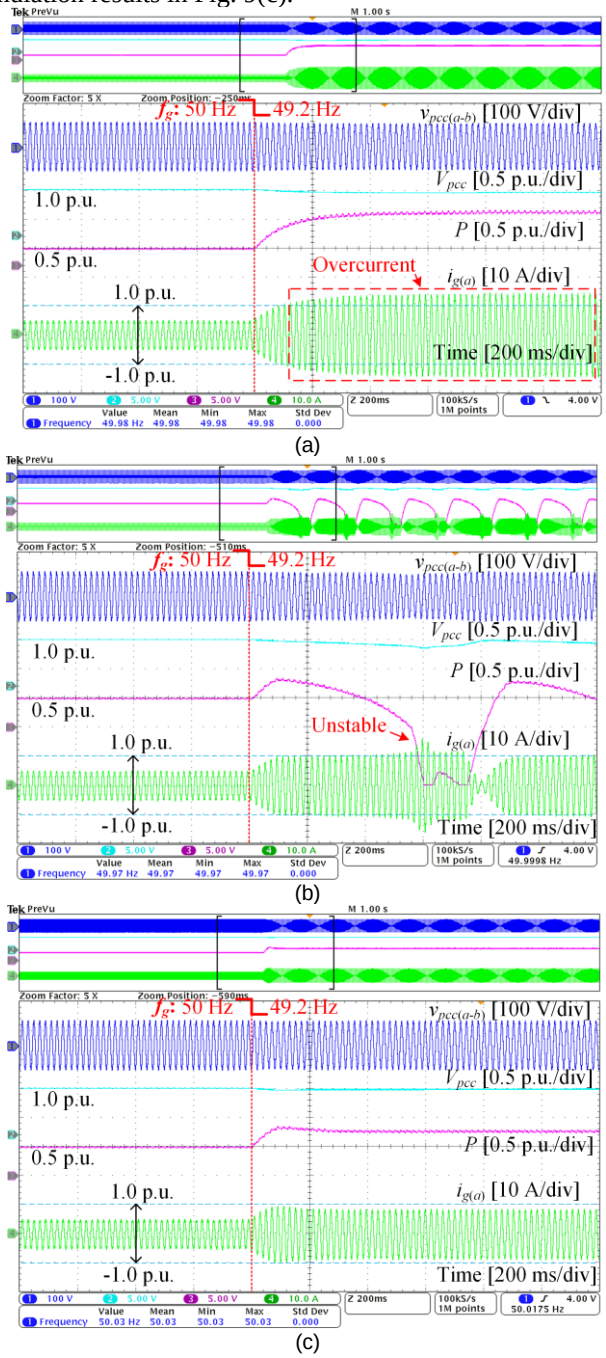

Fig. 12. Experimental waveforms of different current limiting methods under grid frequency drop conditions (Strong grid with SCR=15). (a) Without any limit; (b) With conventional current reference limiting method; (c) With proposed virtual power angle limiting method. (CH1: phase to phase voltage at the PCC; CH2: PCC voltage amplitude, 25 V/div; CH3: active power, 400 W/div; CH4: grid phase current)

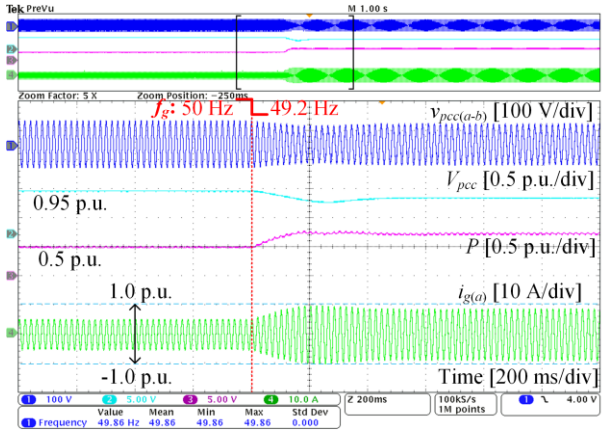

Fig. 13. Experimental waveforms of proposed virtual power angle limiting method under grid frequency drop conditions (Weak grid with SCR=1.5). (CH1: phase to phase voltage at the PCC; CH2: PCC voltage amplitude, 25 V/div; CH3: active power, 400 W/div; CH4: grid phase current)

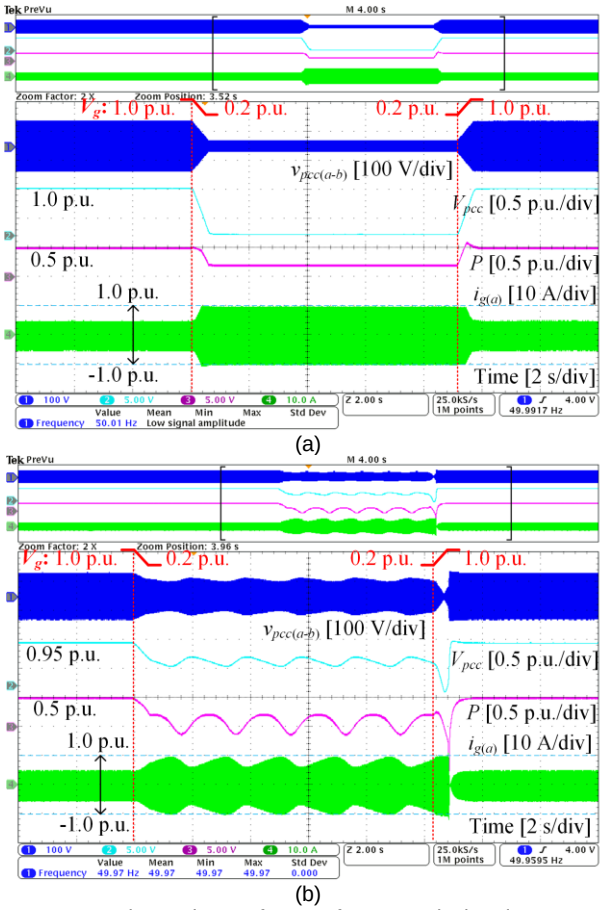

Fig. 14. Experimental waveforms of proposed virtual power angle limiting method under grid voltage sag conditions (Strong and weak grids). (a) Strong grid with SCR = 15; (b) Weak grid with SCR = 1.5. (CH1: phase to phase voltage at the PCC; CH2: PCC voltage amplitude, 25 V/div; CH3: active power, 400 W/div; CH4: grid phase current)

Furthermore, the experimental results of the proposed method under grid frequency drop in weak grids are shown in Fig. 13, where the SCR is equal to 1.5. It can be seen in Fig. 13 that the output current magnitude can also be limited within 1 p.u., which is consistent with the simulation results in Fig. 9(d).

In addition, the experimental results of the proposed method under grid voltage sag conditions are shown in Fig. 14, where the grid voltage magnitude is reduced from 1 p.u. to 0.2 p.u. for around 10 seconds. Same as the simulation, a strong grid case with SCR = 15 and a weak grid case with SCR = 1.5 are used for test. It can be seen in both strong and weak grid cases, the current magnitude can be limited to no more than 1 p.u. effectively by using the proposed method. The experimental results in Fig. 14(a) and (b) agree well with the simulation results in Fig. 10(a) and (b) respectively.

It is worth mentioning that low-frequency oscillations around 0.5 Hz on the PCC voltage magnitude V_{pcc} and active power P can be observed in Fig. 10(b) and Fig. 14(b). This is due to the coupling effect between the inverter output current and the PCC voltage under weak grid conditions. How to eliminate this low-frequency oscillation will be our future research focus.

V. Conclusion

This paper proposes a power-angle-based adaptive overcurrent protection scheme for GFM inverters. By using this proposed method, Both the output power and current can be limited within 1 p.u. stably under large grid disturbances. Thus, the instability problem caused by the conventional current reference limiting method is solved. The proposed method can automatically limit the output current during large grid voltage and frequency disturbances in either strong or weak grids, so the stability and robustness of GFM inverter operating in different grid conditions can be improved. Finally, simulation and experimental results have verified the effectiveness of the proposed method.

References

[1] F. Blaabjerg, Y. Yang, D. Yang, and X. Wang, "Distributed power generation systems and protection," *Proc. of the IEEE*, vol. 105, no. 7, pp. 1311-1331, Jul. 2017.

[2] T. Brown, "Transmission network loading in Europe with high shares of renewables," *IEEE Renew. Power Gener.*, vol. 9, no. 1, pp. 57-65, Jan. 2015.

[3] N. Tleis, *Power Systems Modelling and Fault Analysis - Theory and Practice*, Amsterdam, Netherlands, Elsevier, 2008, ch. 5, pp. 319-345.

[4] N. Hatziargyriou, J. Milanovic, C. Rahmann, V. Ajjarapu, C. Canizares, et al., "Definition and classification of power system stability - revisited & extended," *IEEE Trans. Power Syst.*, vol. 36, no. 4, pp. 3271-3281, Jul. 2021.

[5] X. Wang, M. G. Taul, H. Wu, Y. Liao, F. Blaabjerg, et al, "Grid-synchronization stability of converter-based resources - an overview," *IEEE Open J. Ind. Appl.*, vol. 1, pp. 115-134, Aug. 2020.

[6] H. Xin, L. Huang, L. Zhang, Z. Wang and J. Hu, "Synchronous instability mechanism of P-f droop-controlled voltage source converter caused by current saturation," *IEEE Trans. Power Syst.*, vol. 31, no. 6, pp. 5206-5207, Nov. 2016.

[7] A. Tayyebi, D. Groß, A. Anta, F. Kupzog and F. Dörfler, "Frequency stability of synchronous machines and grid-forming power converters," *IEEE J. Emerg. Sel. Top. Power Electron.*, vol. 8, no. 2, pp. 1004-1018, Jun. 2020.

[8] R. Rosso, X. Wang, M. Liserre, X. Lu and S. Engelken, "Grid-forming converters: control approaches, grid-synchronization, and future trends - a review," *IEEE Open J. Ind. Appl.*, vol. 2, pp. 93-109, 2021.

[9] S. D'Arco and J. A. Suul, "Virtual synchronous machines - classification of implementations and analysis of equivalence to droop controllers for microgrids," in *Proc. IEEE Grenoble Conf.*, 2013, pp. 1-7.

[10] Q.-C. Zhong, P.-L. Nguyen, Z. Ma, and W. Sheng, "Self-synchronized synchronverters: Inverters without a dedicated synchronization unit," *IEEE Trans. Power Electron.*, vol. 29, no. 2, pp. 617-630, Feb. 2014.

[11] H. Bevrani, T. Ise, and Y. Miura, "Virtual synchronous generators: a survey and new perspectives," *Electrical Power Energy Syst.*, vol. 54, pp. 224-254, 2014.

[12] L. Zhang, L. Harnefors, and H.-P. Nee, "Power-synchronization control of grid-connected voltage-source converters," *IEEE Trans. Power Syst.*, vol. 25, no. 2, pp. 809-820, May 2010.

[13] W. Zhang, A. M. Cantarellas, J. Rocabert, A. Luna, and P. Rodriguez, "Synchronous power controller with flexible droop characteristics for renewable power generation systems," *IEEE Trans. Sust. Energy*, vol. 7, no. 4, pp. 1572-1582, Oct. 2016.

[14] D. Groß, M. Colombino, J. Brouillon, and F. Dorfler, "The effect of transmission-line dynamics on grid-forming dispatchable virtual oscillator control," *IEEE Trans. Control Network Syst.*, vol. 6, no. 3, pp. 1148–1160, Sep. 2019.

[15] W. Du, Z. Chen, K. P. Schneider, R. H. Lasseter, S. P. Nandanoori, et al., "A comparative study of two widely used grid-forming droop controls on microgrid small-signal stability," *IEEE J. Emerg. Sel. Top. Power Electron.*, vol. 8, no. 2, pp. 963-975, Jun. 2020.

[16] K. Yu, Q. Ai, S. Wang, J. Ni and T. Lv, "Analysis and optimization of droop controller for microgrid system based on small-signal dynamic model," *IEEE Trans. Smart Grid*, vol. 7, no. 2, pp. 695-705, Mar. 2016.

[17] S. Wang, Z. Liu, J. Liu, D. Boroyevich and R. Burgos, "Small-signal modeling and stability prediction of parallel droop-controlled inverters based on terminal characteristics of individual inverters," *IEEE Trans. Power Electron.*, vol. 35, no. 1, pp. 1045-1063, Jan. 2020.

[18] L. Huang, C. Wu, D. Zhou, and F. Blaabjerg, "Impact of virtual admittance on small-signal stability of grid-forming inverters," in *Proc. 6th IEEE Work. Electron. Grid (eGrid)*, 2021, pp. 1-8.

[19] H. Wu and X. Wang, "A mode-adaptive power-angle control method for transient stability enhancement of virtual synchronous generators," *IEEE J. Emerg. Sel. Top. Power Electron.*, vol. 8, no. 2, pp. 1034-1049, Jun. 2020.

[20] L. Huang, C. Wu, D. Zhou and F. Blaabjerg, "A simplified SISO small-signal model for analyzing instability mechanism of grid-forming inverter under stronger grid," in *Proc. IEEE 22nd Work. Contr. Model. Power Electron. (COMPEL)*, 2021, pp. 1-6.

[21] K. O. Oureilidis and C. S. Demoulias, "A fault clearing method in converter-dominated microgrids with conventional protection means," *IEEE Trans. Power Electron.*, vol. 31, no. 6, pp. 4628-4640, Jun. 2016.

[22] T. Liu, X. Wang, F. Liu, K. Xin and Y. Liu, "A current limiting method for single-loop voltage-magnitude controlled grid-forming converters during symmetrical faults," *IEEE Trans. Power Electron.*, vol. 37, no. 4, pp. 4751-4763, Apr. 2022.

[23] A. D. Paquette and D. M. Divan, "Virtual impedance current limiting for inverters in microgrids with synchronous generators," *IEEE Trans. Ind. Appl.*, vol. 51, no. 2, pp. 1630-1638, Mar.-Apr. 2015.

[24] A. Gkountaras, S. Dieckerhoff, and T. Sezi, "Evaluation of current limiting methods for grid forming inverters in medium voltage microgrids," in *Proc. IEEE ECCE*, Sep. 2015, pp. 1223-1230.

[25] F. Welck, D. Duckwitz, and C. Gloeckler, "Influence of virtual impedance on short circuit performance of virtual synchronous machines in the 9-bus system," in *Proc. Conf. Sustain. Energy Supply Energy Storage Syst. (NEIS)*, Sep. 2017, pp. 1-7.

[26] M. G. Taul, X. Wang, P. Davari, and F. Blaabjerg, "Current limiting control with enhanced dynamics of grid-forming converters during fault conditions," *IEEE J. Emerg. Sel. Top. Power Electron.*, vol. 8, no. 2, pp. 1062-1073, 2020.

[27] L. Huang, H. Xin, Z. Wang, L. Zhang, K. Wu and J. Hu, "Transient stability analysis and control design of droop-controlled voltage source converters considering current limitation," *IEEE Trans. Smart Grid*, vol. 10, no. 1, pp. 578-591, Jan. 2019.

[28] W. Du, R. H. Lasseter and A. S. Khalsa, "Survivability of autonomous microgrid during overload events," *IEEE Trans. Smart Grid*, vol. 10, no. 4, pp. 3515-3524, Jul. 2019.

[29] J. F. Morris, K. H. Ahmed and A. Egea-Àlvarez, "Standardized assessment framework for design and operation of weak AC grid-connected VSC controllers," *IEEE Access*, vol. 9, pp. 95282-95293, 2021.

[30] T. Wen, X. Zou, D. Zhu, X. Guo, L. Peng, and Y. Kang, "Comprehensive perspective on virtual inductor for improved power decoupling of virtual synchronous generator control," *IET Renew. Power Gener.*, vol. 14, no. 4, pp. 485-494, 2020.

[31] B. Fan and X. Wang, “Impact of circular current limiters on transient stability of grid-forming converters,” in *Proc. Int. Power Electron. Conf. (IPEC-Himeji 2022- ECCE Asia)*, 2022, pp. 429-434.